


Article

Intense Cyclones in the Black Sea Region: Change, Variability, Predictability and Manifestations in the Storm Activity

Veronika N. Maslova * , Elena N. Voskresenskaya, Andrey S. Lubkov, Aleksandr V. Yurovsky, Viktor Y. Zhuravskiy and Vladislav P. Evstigneev

Institute of Natural and Technical Systems, Sevastopol 299011, Russia; elena_voskr@mail.ru (E.N.V.); andrey-ls2015@yandex.ru (A.S.L.); a_yurovsky@mail.ru (A.V.Y.); vectorj@mail.ru (V.Y.Z.); vald_e@rambler.ru (V.P.E.)

* Correspondence: veronika_maslova@mail.ru

Received: 24 March 2020; Accepted: 26 May 2020; Published: 1 June 2020



Abstract: Cyclonic activity in the midlatitudes is a form of general atmospheric circulation, and the most intense cyclones are the cause of hydrometeorological anomalies that lead to economic damage, casualties and human losses. This paper examines the features of variability of intense cyclonic activity in the Black Sea region and the examples of their regional manifestations in the storm types. Based on 6-hourly NCEP/NCAR reanalysis data on 1000 hPa geopotential height fields with $2^\circ \times 2^\circ$ spatial resolution and using the methodology by M.Yu. Bardin, objective data were obtained for the identification and estimation of the frequency of deep cyclones (reaching 0.75 and 0.95 quantiles by intensity and depth—intense and extreme cyclones, respectively) for the Black Sea region during the period 1951–2017. Additionally, a specific methodology of more precise cyclone identification based on spherical spline interpolation was successfully applied, and then the two methodologies were compared. The key point of the study is the following: In the background of negative significant linear trends and interdecadal variability (period of about 35 years), typical scales of their interannual variability on the periods of about 2.5–3.5 and 6–8 years were identified. These periods coincide with the time scales of the North Atlantic Oscillation and El Niño–Southern Oscillation, providing an outlook for further study of the patterns of their connection. Besides, seasonal forecasts of frequency of intense cyclones in the Black Sea region were successfully modeled using an artificial neural network technique. Finally, the case studies of regional manifestations of deep cyclones in the types of storms in the northern Black Sea coast revealed substantial differences in the location of deep centers of cyclones and storm tracks associated with the large-scale pressure fields.

Keywords: deep cyclones climatology; decadal–multidecadal variability; interchange of cyclone anomalies; coefficient of determination; Fourier spectrum estimates; artificial intelligence

1. Introduction

Knowledge of the periods and patterns of regional climate variability is important for the development of long-term forecasts of weather and climate anomalies and for solving applied problems of long-term planning of regional sustainable development under climate change [1–3]. Extratropical cyclones in the middle latitudes are responsible for the transfer of heat and moisture, and especially deep ones can have great destructive force due to strong winds [4,5].

According to reanalysis, an increase of global surface temperature is generally accompanied by a decrease in the total number of extratropical cyclones and their packing density in extratropical latitudes of the northern hemisphere, for example in the North Atlantic and European region [6].

However, according to the results of general circulation climatic models, the analysis of the distribution functions of the number of cyclones depending on their intensity revealed an increase in the number of extreme cyclones, particularly in winter over the Atlantic–European region [7]. The frequency of deep cyclones over the northern hemisphere has already doubled during the most recent period of global temperature rise (after 1980) [8]. According to calculations by climatic scenarios of the global warming, the increase of cyclonic activity in the North Atlantic and Western Europe will occur until the end of the 21st century due to an increase in the frequency of cyclones formed over the Gulf Stream and an increase in the transformation of tropical cyclones into extratropical ones, which threaten Western Europe [9,10].

Variability of the Atlantic–European cyclones includes quasiperiodic interannual and decadal scales [11,12]. Cyclones over the northern hemisphere were characterized by a pronounced decadal variability in the rates of deepening and spreading after 1948, while the number of deep cyclones increased on the background of a decrease of the number of small cyclones [13]. At the same time, typical sizes of the total number of cyclones characterized by pronounced interannual fluctuations decreased simultaneously [14]. The quasiperiodic character of variability of the Black Sea region's climate is shown in [15,16] as a change of signs of different hydrometeorological characteristic anomalies: wind speed, wave height, temperature and precipitation. Weather conditions in the Black Sea region, especially in the cold half-year, are associated mostly with cyclonic activity as a part of a large-scale atmospheric circulation [17], while climate anomalies and weather extremes are caused by deep cyclones [10].

This research is a stage of implementation of a greater target of establishing mechanisms and patterns of regional climate variability associated with global processes in the ocean–atmosphere system. At present, it is recognized in scientific literature that these global processes generated in the regions of oceanic gyres and energy-active zones of the World Ocean are responsible for the main scales of regional climate variability [18,19] and their indices can serve as predictors for regional climate anomalies. For example, the storminess in Western Europe, characterized by significant decadal fluctuations and by substantial seasonal and regional differences, is correlated with the North Atlantic Oscillation (NAO) index in separate seasons [20–23] and is determined by the East Atlantic Oscillation phase [24–26], as well as by El Niño–Southern Oscillation positive and negative events [27,28] and different types of El Niño and La Niña [29,30]. The main manifestation mechanism of climate signals, and first of all, NAO, consists of a north–south shift of the North Atlantic storm tracks [31]. A simultaneous increase in the number of cyclones/decrease in their size in the central midlatitude and subpolar Atlantic and a corresponding decrease/increase in the western North Atlantic and the Mediterranean, identified by most reanalyses, indicates a shift of storm tracks to the north over the past decades, confirming the fact that this climatic phenomenon is one of the most significant signals observed in the synoptic dynamics of the atmosphere [32,33].

Extreme cyclones can be explosive as well as nonexplosive, formed under different conditions of large-scale atmospheric circulation. Extreme cyclones in the Atlantic–European region are often “meteorological bombs” [34], with the surface pressure tendency reaching 20 hPa in 6 h [4,5]. Deep cyclones of the Atlantic–European region are supported by interaction with the jet stream and breaking of Rossby waves [35,36], therefore, forming clusters more often than in other cyclogenesis processes [37–39]. Extreme cyclones in the Black Sea region are nonexplosive and not very deep (often no deeper than 980 hPa), but they are characterized by large pressure gradients and high wind speeds of ≥ 30 m/s. One of the most dangerous cyclones in the northern Black Sea region on November 7, 2007, which caused the tanker wreck in the Kerch Strait, had a deepening rate of 5 hPa in 3 h, which was close to those of explosive cyclones [40]. Thus, the extreme cyclones over the Black Sea region are weaker than in the Atlantic–European region, but they can lead to significant damage.

Features of cyclonic activity over the Black Sea region are determined by the geographical position between the Mediterranean region and European territory of Russia. The Mediterranean basin is characterized by seasonality of cyclogenesis mechanisms [41]. In winter, the cyclogenesis process often

starts in series, forming clusters, under the influence of synoptic systems moving from the North Atlantic and interacting with local orography or low-level baroclinicity in the so-called region of the Mediterranean winter cyclone. In spring and especially in summer, thermally caused pressure lows over the land begin to play a major role, the same as such factors as the leeward cyclogenesis of the Atlas mountains in northern Africa and the spread of the Asian monsoon to the east of the Mediterranean region. In contrast to the Mediterranean region, the extreme cyclonic activity of the European territory of Russia is mainly formed by, or associated with, atmospheric circulation in the North Atlantic, while intensification of cyclones over the seas of the European territory of Russia occurs under the influence of local conditions, including topographically induced and convective processes [10].

Earlier, the authors of this paper showed in [42] that most energy of variability of the total number of cyclones in the Black Sea region in 1948–2006 was concentrated at low frequencies (more than 30 years), and after removing the periodicities of more than 20 years, spectral peaks were observed at periods of about 2 and 4 years. Previously, the range of tasks did not include either analysis of the periodicities of the numbers of deep cyclones, which is of greatest practical interest, or their seasonal contribution to the annual spectra. The purpose of this new research was to study variability of the intense cyclonic activity in the Black Sea region in 1951–2017, test an application of an artificial intelligence method to forecasting intense cyclones in the region and identify possible patterns of their association with different storm types generating. The tasks of the study considered in the subsections of the Results and Discussion section include the analysis of annual cycle, time variability of seasonal and annual values of deep cyclones frequency, as well as their standardized anomalies, taking into account both low-frequency and high-frequency components, linear trends and spectral characteristics. Additionally, the approach to forecasting intense cyclones in the Black Sea region using the neural network model was tested. Finally, as an example of regional manifestations of deep cyclones activity, case studies of correspondence of deep cyclones to the types of storminess situations in the northern Black Sea coast were conducted as well.

2. Data and Methods

One of the complexities in the field of cyclonic activity research is a wide variety of applied identification and tracking methods (minimum sea level pressure/geopotential height or maximum vorticity) [43] and data sets, mainly reanalysis (NCEP/NCAR, ERA, JRA, MERRA, 20CR, see acronyms in Table A1) or measurements of atmospheric pressure at stations forming triangles and analyzed in terms of percentiles [21,22,44,45].

Comparison between different cyclone identification and tracking methods and input data was made for example in [32,43,46], in particular for the Mediterranean region [47]. Different methods show different cyclone numbers using the same input data, but there is a good agreement in location of cyclogenesis regions, annual cycles and trends of cyclones. If a standardized value, for example anomalies, is used, statistical regime characteristics are lost, but instead a consensus between different methods on variability, sign and significance of trends is reached. Accordingly, different methods do not constrain the analysis of variability of anomalies of cyclones. As for different input data used, the differences are not only in absolute values of cyclonic activity due to the resolution of the model, but even in the trend estimates both between the measurement and reanalysis data, and between different reanalyses, mainly because of small cyclones [32].

For the Black Sea region within the boundaries 37–50° N, 27–45° E, cyclones were identified and their main parameters were calculated using 4-times daily (6-hourly) NCEP/NCAR reanalysis data [48] for 1951–2017 (<https://psl.noaa.gov/data/reanalysis/reanalysis.shtml>) and the methodology developed by Bardin [49] and approved along with other methods, for example in the international project IMILAST (Intercomparison of Mid Latitude Storm Diagnostic) [43].

A cyclone was identified as a minimum in the 1000 hPa geopotential height field surrounded by closed isohypses with a step of 10 m. The cyclone area was determined by the figure bounded by the

last closed isohypse. Cyclone depth was determined by the difference in geopotential heights between the minimum found at the grid node and the value at the external bounding isohypse. To account for the contribution of the cyclone area to its “power” characteristics, the cyclone intensity (or average depth) was obtained, which is the ratio of the integral cyclone depth to its area.

2.1. Deep, Intense and Extreme Cyclones

Deep cyclones were identified by exceeding the depth or intensity thresholds of 0.75 (upper quartile) and 0.95 quantiles by analogy with the method used for calculating extreme precipitation [50] and storminess by pressure data [21,44]. Correspondingly, the series of deep cyclones were obtained: $Rd75$ (≥ 40 gpm) and $Rd95$ (≥ 90 gpm) by the depth, and $Ri75$ (≥ 16.8 gpm) and $Ri95$ (≥ 33.7 gpm) by the intensity of cyclones, which were called intense ($Rd75$ and $Ri75$) and extreme ($Rd95$ and $Ri95$) cyclones. It is necessary to note that the variability of intense cyclones defined as the 75th percentile includes the variability of extreme ones defined as the 95th percentile.

The frequency (dimensionless quantity) of intense and extreme cyclones was determined as the number of centers of cyclonic systems over the Black Sea region exceeding a given threshold (0.75 and 0.95 quantiles) by depth or intensity for a certain period to the total number of times analyzed (equal to the number of days in a period multiplied by 4 times because 6-hourly daily data were used).

Variation of deep cyclones was analyzed in the following terms:

- Comparison of seasonal and annual mean values;
- Annual cycle of long-term monthly mean and dispersion of the frequency of deep cyclones;
- Long-term variability of seasonal and annual frequency of deep cyclones and their anomalies normalized on standard deviation σ ;
- Linear trends and their p -value with contribution to dispersion (determination coefficient R^2);
- Variability of low-frequency (≥ 14 years) and high-frequency (< 14 years) components of seasonal and annual series with the assessments of contribution to dispersion;
- Spectral Fourier analysis of high-frequency component (< 14 years) of seasonal and annual frequency of deep cyclones.

2.2. Additional Methodology and Intercomparison of Data Sets

At the same time, a specific methodology [51] of cyclone identification on the basis of spherical spline interpolation was involved in the research for the case studies in Section 3.5. It was done after we had obtained the following result: about 30% of extreme storms in the region were caused by shallow local cyclones occurring over the Black Sea, some of which could not be identified using the method [49] because of a coarser isohypse step. The cyclone tracking algorithm consisted of 3 stages: finding a minima for baric formations in a coarse grid; transferring the pole of the spherical coordinate system into the low pressure center and spherical spline interpolation [52] in order to obtain geometry characteristics of cyclone; combining the low-pressure centers into a single cyclone event at a given distance. To find centers of low pressure, the geopotential data at levels of 1000 hPa (Z_{1000}) and 500 hPa (Z_{500}) were recalculated into sea level pressure (SLP) according to Equation (1):

$$SLP = 1000e^{Z_{1000}/(1.5422885(Z_{500}-Z_{1000}))}. \quad (1)$$

The procedure of low-pressure center search in a coarse grid was as follows: if during sequential considerations of each grid node SLP increased in 4 directions, the starting point was identified as a minimum of SLP field. Next, the pole of the spherical coordinate system was transferred into the center of low pressure, after that subsequent interpolation was performed using spherical splines. Then a closed isobar was found sequentially in 36 directions from the center of a cyclone. Thus, the average radius, pressure gradient and the cyclone area were calculated. The depth of the cyclone was estimated as the SLP difference between its center and the last closed isobar. Then, the identified low-pressure

centers were combined into a single cyclone if the distance between their centers did not exceed 500 km at the same time (every 6 h).

Good quality of both methods used was determined by their comparison in Figure 1. The curve of density probability of deviations between baric systems in the data sets is shown in Figure 1a for thousands of kilometers. The probability density tends to zero for deviations of more than 500 km. Figure 1b shows the number of deviations between the two data sets up to 200 km in more detail. According to it, the maximum repeatability was observed in the deviation range of 20–25 km.

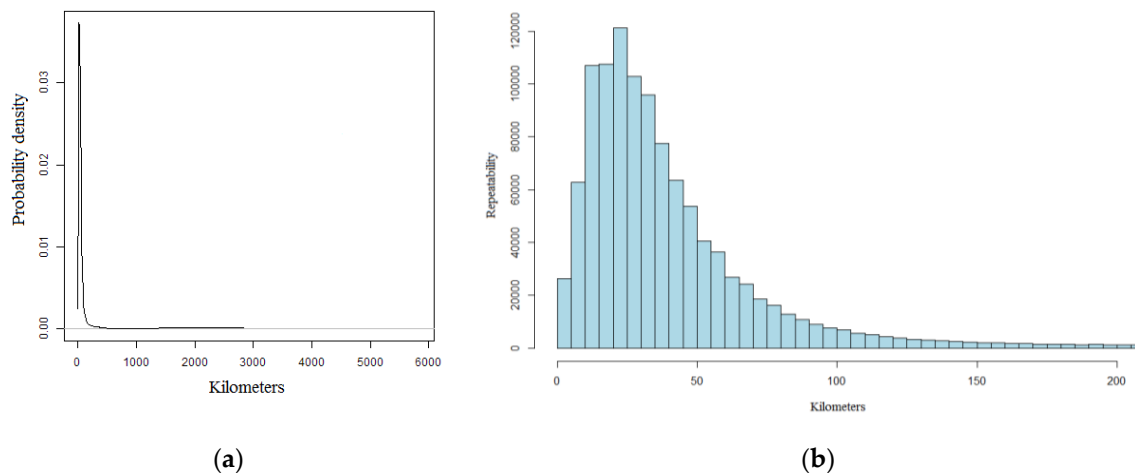


Figure 1. Results of statistical comparison of baric formations using data set #1 after [49] and the specific data set #2 after [51]: (a) the curve of density probability of deviations between baric systems in compared data sets; (b) histogram of repeatability of deviations between baric formations in compared data sets on 0–200 km spatial scale.

2.3. Spectral Analysis

To determine the periods of variability of deep cyclones in the Black Sea region, a spectral Fourier analysis of seasonal and annual values of the frequency of cyclones was carried out [53]. To obtain the spectra estimates, the Parzen window was used for averaging periodograms [54]. The window width was taken equal to 20 with the number of frequency points being 100. A linear trend for the period 1951–2017 was previously removed from the series of frequencies of deep cyclones. Then, a high-frequency filtering with periods of up to 14 years was applied to the residuals of the detrending procedure because it was not possible to determine reliable spectral peaks during longer periods for a 67-year time interval.

2.4. Neural Network Model

An approach of modeling and forecasting time variability of intense cyclones in the Black Sea region was tested using the method of artificial neural network. A set of monthly average climate indices was used as input parameters in the neural network model consisting of the indices of large-scale signals of the ocean–atmosphere system in the northern hemisphere [18,55], southern hemisphere [56] and equatorial zone (Southern Oscillation index) [57]. These indices were calculated as a difference in pressure or geopotential height between the centers of action of these signals using the monthly average NCEP/NCAR reanalysis fields [48] on the 500 hPa geopotential height and SLP for the period 1948–2019 with a spatial resolution of $2.5^\circ \times 2.5^\circ$. The indices were calculated and calculations were carried out for each month separately, thereby eliminating seasonal variability. Linear trends of the indices were excluded for the whole period.

To simulate the frequency of intense cyclones in the Black Sea region, a unidirectional heteroassociative single-layer (one hidden layer) neural network with a teacher was used [58]. The neurons of the input, hidden and output layer were represented by a sigmoidal bipolar function

$\tanh(\beta x)$. The model assimilated data until 2006 within the 1951–1975 training period and 1976–2006 testing period. After that, there was a period of modeling/predicting cyclones and the validation was made for the 2007–2017 control period.

The learning was based on the backpropagation algorithm according to [59]. The aim of the learning was to determine the neuron weights of each layer in such a way that for a given input vector it could be possible to obtain output values coinciding with the expected values of the training sample with the required accuracy [58]. In the classical statement of the task, the maximum learning is determined by the objective function calculated at each step of the training sample and is defined usually as a quadratic sum of the differences between the actual and expected values of the output signal [58,59]. When it is impossible to achieve coincidence between model calculations and known values with the required accuracy, the maximum learning is defined as the minimum of the objective function [58]. In this study, the training sample consisted of only 30 values, which complicated the determination of the maximum learning by classical method. In this regard, to determine the maximum learning, the method from the paper [60] was used, which was as follows: Correction of the weights of neurons was carried out using the classical objective function, but the training sample was repeated many times, while the values of the weights were saved. At each iteration of the training, the correlation coefficients with the training (r_{study}) and test (r_{test}) samples were calculated. The learning maximum had to satisfy 2 conditions: determining the iteration of the learning with the maximum r_{study} and the inequality $|r_{study} - r_{test}| < 0.15$ had to be satisfied. If the second condition was not fulfilled, the closest iteration corresponding to both conditions was taken as the maximum learning. Since a test sample was used in the search for learning maximum, it was necessary to use an independent control sample for an objective assessment of the model capabilities.

The adaptation of the model was carried out by analogy with the paper [61] and included the stages of preprocessing, modeling and postprocessing. At the stage of preliminary data processing, a search was made for the correlation relationships between the frequency of intense cyclones and the values of the indices of large-scale signals in the previous 2, 4 and 6 months, after that the input parameters having the greatest relationship with the prognostic parameter were selected for the model operational work. At the modeling stage, the model was launched using, at the input, all possible combinations of indices selected at the preliminary stage with different numbers of hidden layer neurons. After training for each such neural network, correlations of model calculations with the results of the test and training samples were remembered. At the final stage, the best 20 neural network combinations were selected based on a ranking of correlation coefficients at a test sample. Then, their ensemble was calculated, the quality of which was estimated in comparison with the control sample.

2.5. Material for Case Studies Involving the Types of Storms

Regional manifestations of deep cyclones were studied for the selected large-scale stormy atmospheric situations in the northern Black Sea coast identified earlier in [15]. On the basis of the objective method of cluster analysis applied to observational hydrometeorological data, four types of stormy atmospheric situations (including 2 subtypes) associated with different wave heights in the northern Black Sea coast were identified. They represented four types of meridional circulation: type 1 (western), type 2 (mixed), type 3 (central) and type 4 (eastern). In addition, two subtypes were identified for the types 1 and 2 (western and mixed), for which the macrosynoptic conditions were significantly different. The northwest transfer of air masses was carried out for the subtype 1a of the western type and the northeastern/eastern for the subtype 1b. Similarly, the mixed type 2, dependent on the location of the pressure ridges relative to the Azov-Black Sea basin, was represented by two subtypes: the transfer of air masses carried out from the south to the Black Sea for the subtype 2a and from the north/northwest for the subtype 2b.

Although these types of storminess are based on the features of regional climatic manifestations, they do not contradict the types of large scale atmospheric circulation patterns over midlatitudes of the

northern hemisphere and Central Europe originating from Katz's classification [62], Wangenheim-Girs's classification [63,64] with modifications [65], Grossweterlagen's classification [66–68] or types of synoptic situations with deep cyclones in central Europe [69].

Only those types with wave height higher than or equal to 5 m were selected and used as a range of data for daily composite analysis, they were 1b with 13 events, 2a with 17 events, 2b with 10 events and type 3 with 5 events (Table 1).

Table 1. Dates of storms (day.month.year) with a wave height higher than or equal to 5 m associated with one of the types of atmospheric processes according to [15] used for composite analysis.

Type 1b (Western Type b)	Type 2a (Mixed Type a)	Type 2b (Mixed Type b)	Type 3 (Central Type)
29.09.1959	18.10.1958	26.01.1964	06.01.1969
24.01.1961	20.01.1960	26.11.1964	10.03.1970
13.02.1962	21.11.1960	03.04.1965	18.11.1970
05.01.1965	15.02.1962	28.01.1967	05.02.1972
07.01.1965	21.02.1963	17.01.1968	29.08.2006
06.01.1966	12.01.1968	28.10.1969	
15.01.1966	14.07.1969	04.02.1970	
09.01.1967	18.12.1969	23.10.1971	
12.02.1967	24.05.1970	26.12.1971	
20.02.1979	20.09.1971	06.01.1976	
10.11.1981	06.08.1972		
16.11.1981	27.02.1973		
13.02.2011	01.12.1973		
	18.12.1981		
	03.03.1988		
	11.12.2007		
	27.12.2007		

Due to the limited number of storm events for each type of large-scale circulation regime, a case study approach was used to analyze regional manifestations of deep cyclones. For the range of dates for each selected type of stormy atmospheric situations with a wave height higher than or equal to 5 m, composite maps of the following parameters were obtained:

- Centers of cyclones in the days of storms based on data set #1 after [49];
- Full storm tracks of cyclones based on data set #2 after [51], the centers of which were over the Black Sea region on the composite dates;
- 3–6. Sea level pressure; 1000 hPa and 500 hPa geopotential height; 1000 hPa wind vector.

Two data sets based on the methodologies by M.Y. Bardin [49] (data set #1) and the current authors' methodology of objective tracking [51] (data set #2) were compared and used to construct composite maps of cyclones to ensure the reliability of results. Other composite maps were obtained using an interactive tool for plotting daily mean composites on the basis of NCEP/NCAR reanalysis data, available at <https://www.esrl.noaa.gov/psd/data/composites/day/>.

3. Results and Discussion

3.1. Annual Cycle of Long-Term Mean Characteristics of the Frequency of Deep Cyclones

First, let us consider and compare the mean values and the spread of values (standard deviation σ) of the frequency of the identified series of deep cyclones by seasons and months. As for the total number of cyclones in the region, an increase was expected in winter and a decrease in summer [42].

Comparison of the seasonal (conventional seasons) and annual frequency of the series of deep cyclones can be seen in Figure 2. The frequency of deep cyclones determined by the depth was higher

annually and in all seasons than that identified by the intensity, because the depth of cyclones does not take into account their area (and consequently a gradient) in contrast to intensity. As expected, the highest values of the frequency of deep cyclones were in winter (with a maximum in February) while the lowest ones were in summer (with the minimum in August). Mean winter values of the frequency of intense cyclones were 6–8 times higher than summer values, 2.3–2.5 times higher than autumn values and 1.2–1.3 times higher than spring values. The frequency of extreme cyclones in winter was 2.4–2.8 times higher than that in spring and more than 3.5 times higher than that in autumn. Long-term mean of the summer frequency of extreme cyclones in the 1951–2017 period was close to zero (from May to August) because such cyclones are observed only in certain years.

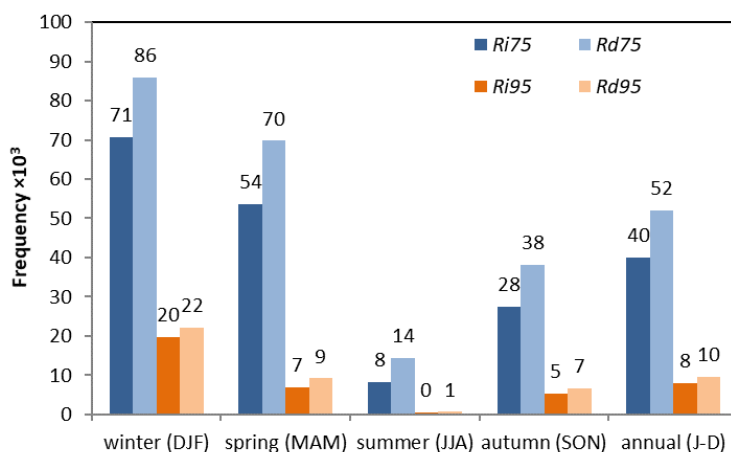


Figure 2. Seasonal and annual values of the frequency of intense ($Ri75$ and $Rd75$) and extreme ($Ri95$ and $Rd95$) cyclones in the Black Sea region. Data signatures are rounded values.

The annual cycle on a monthly basis was similar to both intense ($Ri75$ and $Rd75$) and extreme ($Ri95$ and $Rd95$) cyclones by their long-term mean values and standard deviations (Figure 3). The feature of the annual cycle of extreme cyclones (Figure 3b,d) was a steeper descending slope from winter to spring months, resulting in the highest activity of these cyclones from November to March (while for intense cyclones this period was from November to May). As for intense cyclones (Figure 3a,c), September violated the monotonic increase from summer to winter, characterized by a peak of long-term mean values and standard deviations. The long-term mean values of intense cyclones were higher than the standard deviation from November to April, which indicates that the values tended to be closer to the mean these months, and lower from May to October, when the values were spread out over a wider range.

A feature of intense cyclones was that the largest spread of the values (σ) relative to the mean was observed in January (Figure 3a,c), while the mean values (M) of the time series of both intense and extreme cyclones and standard deviation of extreme cyclones were in February (Figure 3). That is, in January, the mean values can be less predictable for intense cyclones than, for example, in February, as well as in September for the same reasons described above. This feature is also noted in the Section 3.4. As for extreme cyclones (Figure 3b,d), the standard deviation was higher than the mean values during all months. In this regard and due to low values of frequencies, we did not try to simulate extreme cyclones using the neural network model.

The maximum frequency of the deep cyclones of the Northern hemisphere was also shown in February in [8]. In addition, in the paper [8], the maximum frequency of deep cyclones also shifted to the spring months in recent decades, i.e., the deepest cyclones were observed in January and February before the most recent period of global temperature rise (after 1980), and after that the deepest cyclones were observed in February and March. In this research, conducted throughout the entire period 1951–2017, it is noted that mean long-term frequency values of intense cyclones ($Ri75$ and $Rd75$) were

similar in January and March, with the dominance in March; while for the frequency of extreme cyclones ($Ri95$ and $Rd95$), January substantially prevailed over March.

Due to the strong correlation (0.9–0.99) between the frequency of deep cyclones identified by the depth and intensity ($Rd75/95$ and $Ri75/95$), and taking into account that intensity is a more complex parameter concerning both depth and area of cyclones, we further understand intense and extreme cyclones as those deep cyclones which were identified by the intensity (respectively, $Ri75$ and $Ri95$).

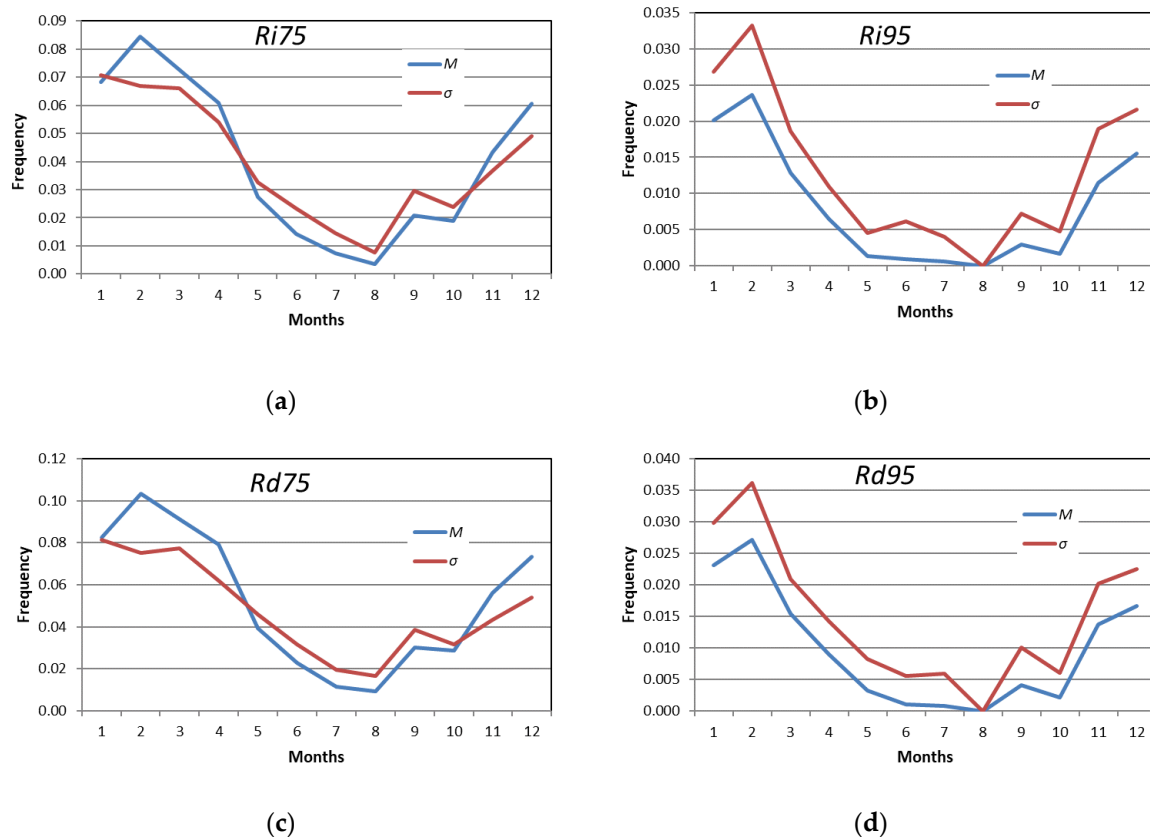


Figure 3. Annual cycle of long-term mean values (M) and standard deviations (σ) of the frequency of deep cyclones in the Black Sea region: (a,c) Intense cyclones ($Ri75$ and $Rd75$); (b,d) Extreme cyclones ($Ri95$ and $Rd95$).

3.2. Variability, Trends and Anomalies of Seasonal and Annual Frequency of Deep Cyclones

This subsection is devoted to long-term variability of the seasonal (Figure 4a,b) and annual (Figure 4c,d) frequencies of intense and extreme cyclones in the Black Sea region for the period 1951–2017 and their anomalies normalized by standard deviation (Figure 5).

The most prominent feature of variability of annual frequencies of intense and extreme cyclones (Figure 4c,d) was a peak in the mid-1960s, mainly due to winter and spring contributions (Figure 4a,b), followed by a descent until the 1990s and a period of increase after that up to the end of the time interval. A secondary increase in winter frequency of both intense and extreme cyclones (Figure 4a,b) was found at the beginning of the time interval and after 2000. Autumn frequencies of deep cyclones were low or negligible in the 1980s.

Variability of annual extreme cyclones (Figure 4d) is characterized by a greater contribution of interannual amplitude than that of intense cyclones (Figure 4c). Figure 4c,d shows negative linear trends of the annual frequency of both intense and extreme cyclones, which are significant at the level of 97.5% for intense cyclones and of 92.4% for extreme cyclones (according to Table 2 described below). Variability of 14-year low-frequency filtration residues of annual values (Figure 4c,d) demonstrates an interdecadal period of about 35 years. The significance of this period is not possible to determine using

the 67-year data set (1951–2017); however, it is clear that contribution of low-frequency variability to the variance reached significant values, so it was evaluated further using the coefficient of determination R^2 (see Table 2).

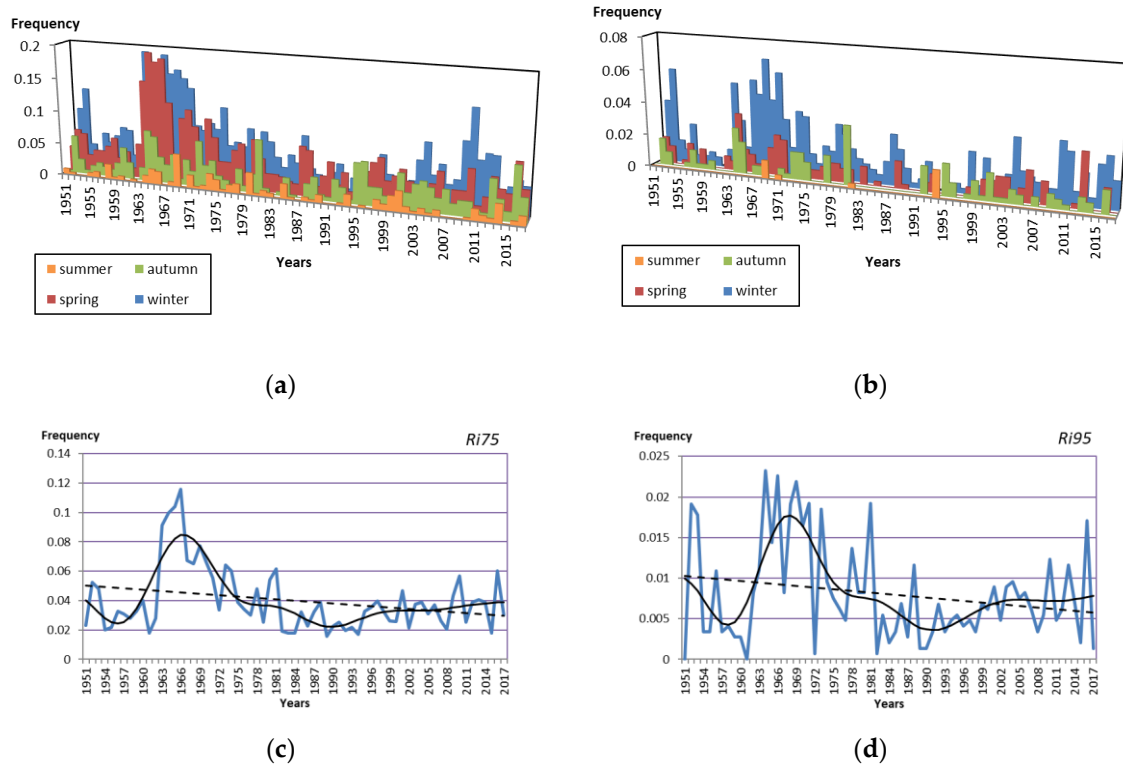


Figure 4. Long-term variability of (a,b) seasonal and (c,d) annual frequencies of intense ($Ri75$, left) and extreme ($Ri95$, right) cyclones in the Black Sea region, linear trend (dashed line), low-frequency part of the variability after filtration ≥ 14 years (curved line).

Table 2. Coefficients of linear trends of seasonal and annual frequency of deep cyclones (k_{lin}) and the significance of error (p -value). Estimates (in %) of contribution (determination coefficients R^2) to the dispersion of seasonal and annual frequency of intense ($Ri75$) and extreme ($Ri95$) cyclones: contribution of the linear trend (R^2_{lin}); contribution of the low-frequency component without the linear trend ($R^2_{\geq 14}$); contribution of the low-frequency component taking into account the linear trend (R^2_{low}); contribution of the high-frequency component (R^2_{high}).

Frequency Parameter	k_{lin}	p -Value	R^2_{lin}	$R^2_{\geq 14}$	$R^2_{low} = R^2_{\geq 14} + R^2_{lin}$	$R^2_{high} = 100 - R^2_{low}$
<i>Ri75</i>						
winter	-6.783×10^{-4}	0.0105	9.61	51.84	61.45	38.55
spring	-6.064×10^{-4}	0.0145	9	43.56	52.56	47.44
summer	$+7.591 \times 10^{-7}$	0.9903	0	15.21	15.21	84.79
autumn	$+8.299 \times 10^{-5}$	0.5256	0.64	17.64	18.28	81.72
annual	-3.058×10^{-4}	0.0251	7.29	53.29	60.58	39.42
<i>Ri95</i>						
winter	-1.990×10^{-4}	0.0535	5.76	42.25	48.01	51.99
spring	-3.893×10^{-5}	0.4423	1	14.4	15.4	84.6
summer	-1.627×10^{-6}	0.9158	0.01	12.96	12.97	87.03
autumn	-2.138×10^{-5}	0.6546	0.36	9	9.36	90.64
annual	-6.824×10^{-5}	0.0758	4.84	33.64	38.48	61.52

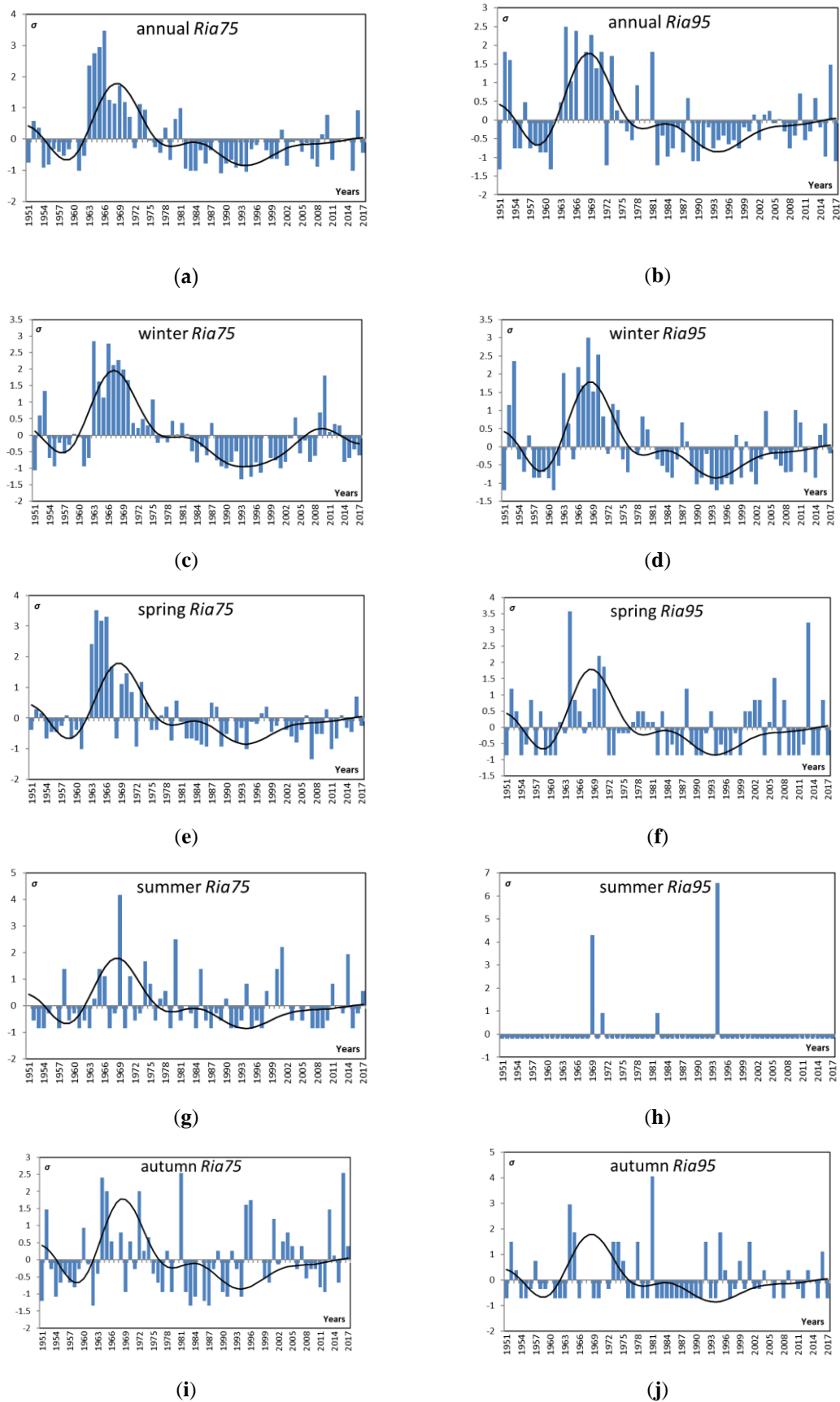


Figure 5. Standardized anomalies (*Ria*, σ) of the frequency of (a,b) annual and (c–j) seasonal deep cyclones: intense (*Ria75*, left) and extreme (*Ria95*, right). The curve represents ≥ 14 years filtering residuals.

Now, let us specify the intervals and relative values of the periods of low-frequency variability identified in Figure 4 in terms of standardized anomalies (normalized by standard deviation σ) of intense and extreme cyclones referred to as *Ria75* and *Ria95* (Figure 5). A period of positive anomalies of annual frequency of the intense cyclones (Figure 5a), with some of them exceeding 3σ , was observed in 1960–1975, while the rest of the time interval was characterized by negative anomalies, with the strongest ones more than 1σ . A slightly shifted period of positive anomalies of annual extreme cyclones (Figure 5b), with a maximum reaching 2.5σ , was observed in 1962–1977, and the rest was characterized by negative anomalies with the module up to about 1σ , except for a couple of years at the beginning of the time interval (1951) that had weak positive anomalies. The character of interdecadal variability of winter anomalies of extreme cyclones (Figure 5d) and spring anomalies of intense cyclones (Figure 5e) was in good agreement with the corresponding annual anomalies (Figure 5a,b). As for the winter anomalies of intense cyclones (Figure 5c), their interdecadal variability differed from the annual variability by the period of positive anomalies in 2006–2013. Peculiarity of the interdecadal variability of spring and autumn anomalies of extreme cyclones (Figure 5f,j) and autumn and summer anomalies of intense cyclones (Figure 5g,i) was characterized by the period of positive anomalies around 2000, and further by negative anomalies and again positive ones (for intense cyclones) or transitioning to positive (for extreme cyclones) at the end of the time interval (2017). Summer anomalies of extreme cyclones were negligible (Figure 5h).

This clearly anomalous period approximately from the mid-1960s to the mid-1970s, with a notable maximum in the number of cyclones, was found both in depth and intensity of the total number of cyclones over the Black Sea region on shorter time series in earlier papers [23,42,70], as well as in the frequency of wave heights [15] and water temperature (on the surface and 100 m horizon) [71]. This and other periods of intensification of deep cyclones are consistent with the periods of increasing and decreasing storm activity in the Black Sea region identified in the papers [15,72–76]. The authors of the paper [72] found the period of positive standardized frequency anomalies of the northern hemisphere cyclones at low latitudes from the mid-1960s to the mid-1970s and the period of negative anomalies in the 1990s. The greatest number of storms caused by cyclones was observed in the west of the Black Sea region in the 1960s and after the year 2000 [74], and off the coast of the Danube Delta in the late 1960s, 1970s and 1990s [75]. Besides that, we found earlier that cyclonic activity (total number of cyclones) was characterized by the following patterns over the Black Sea region: an increase in the frequency of winter cyclones over the central and southern parts of the sea in the 1980s and 1990s, while in the 1960s and 2000s the maximum frequency of cyclones moved to the land to the northern part of the Black sea region, while an increase of frequency of winter anticyclones over the southwestern part of the sea was observed. The results obtained further in Sections 3.4 and 3.5 confirmed that these anomalous episodes shown in the frequency of intense cyclones can be explained by atmospheric dynamics on a regional and global scale.

It can be supposed that the end of the time interval (2017) was characterized by the transition from negative to positive annual anomalies of the frequency of deep cyclones (Figure 5a,b) on the background of the sustainable growth of the interdecadal variability of anomalies. Besides, if recent years have been characterized by an increase in the surface temperature of the Black Sea, then the paper [77] based on numerical experiments on the sensitivity of the regional atmospheric circulation to the sea surface temperature can be referred to. It showed that additional cyclonic vorticity originates in both winter and summer central months for the case of a warm sea [77]. The analyses of long-term variability of the Black Sea surface temperature and intermediate 100 m layer water temperature for the interval 1951–2017 [71] confirmed the presence of interdecadal temperature variations with a period of 40–50 years and an amplitude of up to $0.8\text{ }^{\circ}\text{C}$, while a common trend representing a sharp rise in temperature over the past 20 years was identified for both horizons.

Table 2 shows the coefficients of linear trends of seasonal and annual frequency of deep cyclones (k_{lin}) with the significance of error (p -value), as well as the contribution of high-frequency (up to 14 years) and low-frequency (≥ 14 years) components of variability, taking into account and without

taking into account the linear trend, to the dispersion of the frequency of deep cyclones. As mentioned above, significant linear trends of the annual frequency of deep cyclones have a negative sign. As for the seasons, significant negative coefficients were identified for the frequency of intense cyclones at the level of more than 98% in winter and spring, and for the frequency of extreme cyclones only in winter at the level of 94.6%. Estimates of the contribution of linear trends (R^2_{lin}) to the dispersion of the annual frequencies of intense and extreme cyclones were 7.3% and 4.8%, in particular due to winter and spring: respectively, 9.6% and 9% for intense cyclones and 5.8% and 1% for extreme cyclones.

The trends found for deep cyclones support the tendencies identified in earlier works for the total number of cyclones in the Black Sea region. For example, the paper [23] showed that the frequency of cyclones decreased in all seasons (except summer) as a result of the intensification of the North Atlantic Oscillation in the 1960–1990s and the displacement of the predominant paths of synoptic disturbances to the north.

The contribution of the low-frequency component to the annual values, without taking into account the linear trend ($R^2_{\geq 14}$), was more than 53% for the frequency of intense cyclones (mainly due to winter and spring) and more than 33% for the frequency of extreme cyclones (due to winter).

Taking into account the linear trend, the low-frequency variability ($R^2_{low} = R^2_{\geq 14} + R^2_{lin}$) explained more than 60% and 38% of the dispersion of annual frequency of intense and extreme cyclones, respectively, due to the winter season, as well as spring in the case of intense cyclones. The revealed linear and quasiperiodic tendencies could be both an indicator of global warming and part of the lower-frequency variability in the ocean–atmosphere system determined by climate signals of the Atlantic and Pacific oceans [72,78].

As for the contribution of high-frequency variability ($R^2_{high} = 100 - R^2_{low}$) to the standard deviation of the frequency of intense and extreme cyclones, a summer–autumn maximum of 81–96%, as well as a spring one for extreme cyclones, was noted, while the contribution of high-frequency variability to the annual values reached 39.4% and 61.5%, respectively.

3.3. Spectral Analysis of the High-Frequency Component of Deep Cyclones

Figure 6 presents averaged periodograms of annual and seasonal values of the high-frequency component of deep cyclones in the Black Sea region. The spectra of the annual frequency of intense cyclones were characterized by peaks at 7.7 and 3.4 years and a secondary peak at 2.5 years. For annual values of extreme cyclones, spectral peaks stood out at 5.6, 3.4 and 2.4 years. Herewith, a descending spectrum was observed for intense cyclones, and an ascending one for extreme cyclones, which confirms the previously mentioned feature: for extreme cyclones, more energy is concentrated at higher frequencies (shorter periods), and for intense cyclones at lower frequencies (longer periods).

The main contribution to the energy of the annual spectra of the high-frequency component of intense cyclones was made by spring, as well as winter, peaks and to a lesser extent by autumn peaks (Figure 6a). As for extreme cyclones, winter spectra made the main contribution to the energy of annual spectra, and the energy of autumn and spring spectra was approximately equal. Close spectral peaks of the high-frequency component of deep cyclones by seasons were identified in the following range of years:

- For the frequency of intense cyclones (Figure 6b), 7.4–8.3 in spring and autumn, 5.12–5.7 in winter and summer, from 3.4–3.5 in winter and spring to 3.8 in autumn, and also 2.7 in summer (notably, lower-frequency peaks in the winter-spring period and higher-frequency peaks in the summer-autumn period have higher energy).
- For the frequency of extreme cyclones (Figure 6c), 5.6, 6.3 and 7.7 in winter, spring and autumn, respectively, and from 3.4 in winter and autumn to 2.5 in spring (summer spectral peaks are insignificant due to the small number of extreme cyclones in this season).

The periods of variability of the frequency of deep cyclones in the Black Sea region identified by spectral analysis were also typical for the global processes in the ocean–atmosphere system, such as the

North Atlantic Oscillation—NAO (2.4; 4.8; 7.7 years for the winter index) [79] and El Niño–Southern Oscillation—ENSO (3–4 and 7–8 years) [78]. Thus, the results obtained confirmed that the indicated climatic processes can be responsible for the interannual variability of the frequency of deep cyclones in the Black Sea region. Earlier, we showed in [42] that correlation coefficients of the winter–spring parameters of the total number of cyclones in the Black Sea region exceeded 0.6 with NAO indices, while they reached 0.49 with Southern Oscillation indices at time lags of 4–6 months, and the joint influence of NAO and ENSO significantly exceeded 50% of the interannual variability of cyclones in the studied region. That is why a similar correlation is expected with deep cyclones identified by quantiles. It can be a purpose of our further study.

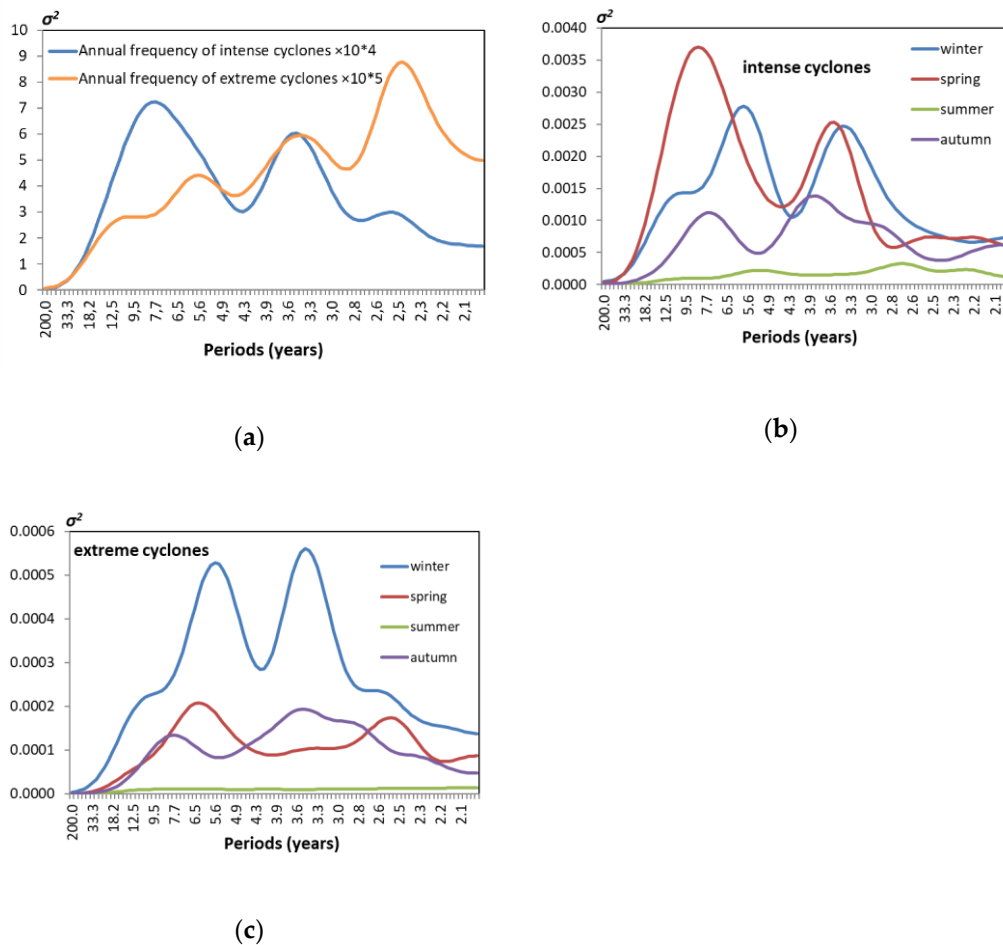


Figure 6. Averaged periodograms of (a) annual and (b,c) seasonal values of the high-frequency component of the frequency of (b) intense and (c) extreme cyclones in the Black Sea region.

3.4. Approach to Forecasting Intense Cyclones in the Black Sea Region Using the Neural Network Model

Long-term forecast (with a lead time from a month to a year) is an unresolved recent problem. The requirements for the quality of such forecasts still cannot be achieved using modern global climate models. At the same time, the need for high-quality long-term forecasts not only persists, but also becomes more relevant.

A model based on the method of artificial neural network to forecast the frequency of intense cyclones was tested in this paper. Previously, such a modeling approach was successfully applied to predict anomalies in the Niño3.4 region, with a lead time from 1 to 9 months [61]. SLP fluctuations in the centers of action of the global atmosphere are used as predictors in the model.

The ability of the neural network model to project the frequency of intense cyclones for each month separately with different lead times of 2, 4, and 6 months was tested in this paper. For the control

period (2007–2017), standard deviations, correlation coefficients and root mean square error (RMSE) were calculated, and Taylor diagrams normalized to standard deviations were obtained (Figure 7). The critical value of the statistically significant correlation for a series of 11 values (from 2007 to 2017) being 0.45 (at $p = 0.01$) was considered as a threshold for the reliable result—all calculations with a correlation below this threshold were considered unreliable.

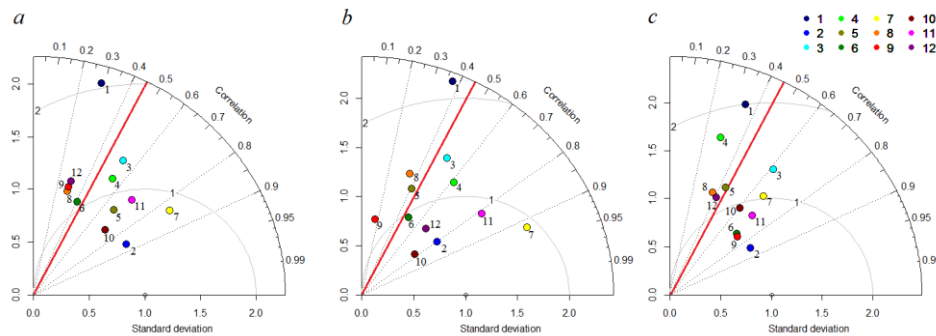


Figure 7. Taylor diagrams normalized to the standard deviation for the monthly (1–12) frequency of intense cyclones in the Black Sea region according to the forecast for (a) 2, (b) 4 and (c) 6 months for the period of the control sample (2007–2017). Red line is the critical value of the statistically significant correlation being 0.45 (at $p = 0.01$).

Equally good reproducibility of the projected parameter of the model was shown for October, November, February and July (the correlation, r , was 0.7–0.95 and normalized RMSE, $RMSE/\sigma$, was 0.40–0.65 for October, February and July, and 0.63–0.80 for November), but for July the estimate was biased, since only a few cases of intense cyclones were identified over the Black Sea region during the control period, in 2014, 2016 and 2017. A model with a lead time of 2 months (Figure 7a) reproduced the projected parameter somewhat worse in March, April and May ($r = 0.55$ –0.65, $RMSE/\sigma = 0.54$ –0.67), while in January, June, August, September and December the modeling quality was unsatisfactory ($r < 0.45$, $RMSE/\sigma = 0.87$ –1.01). A model with a lead time of 4 months (Figure 7b) satisfactorily reproduced March, April, June and December ($r = 0.48$ –0.68, $RMSE/\sigma$ is 0.54 for December and 0.65–0.84 for March, April and June). At the same time, the correlations in January, May, August and September were outside the threshold of significance ($r < 0.45$, $RMSE/\sigma = 0.7$ –1.13). A model with a lead time of 6 months (Figure 7c), for the above mentioned November, February and July, also had high simulation quality for June and September ($r = 0.74$ –0.88, $RMSE/\sigma = 0.64$ –0.7). A satisfactory quality of modeling was noted for March ($r = 0.61$), and unsatisfactory for January, April, May, August and December ($r < 0.45$, $RMSE/\sigma = 0.64$). Months with an unsatisfactory forecast can be explained by a different set of predictors (climatic signals) for different lead times, as well as by a large standard deviation of the values, as mentioned in Section 3.1.

A comparison of the quality of the modeling of the annual time series of the frequency of intense cyclones for different lead times was drawn from Figure 8. The correlations between calculated and simulated frequency of intense cyclones for lead times 2 (see Figure 8a), 4, (see Figure 8b) and 6 (see Figure 8c) months were 0.66, 0.66 and 0.69, respectively, and RMSEs were 0.039, 0.039, and 0.037 with an average deviation of 0.061.

According to Figures 7 and 8, the model with a greater forecast lead time (6 months) appears to have been slightly better than models with lower lead times (2 and 4 months). It requires further study because the found feature may be associated with a typical period of manifestation of the global climate signal El Niño–Southern Oscillation, which is about 6 months for the Atlantic–European region [30,80,81]. After this time, the mature phase of ENSO and the responding rearrangement of the global atmospheric circulation develop [82,83].

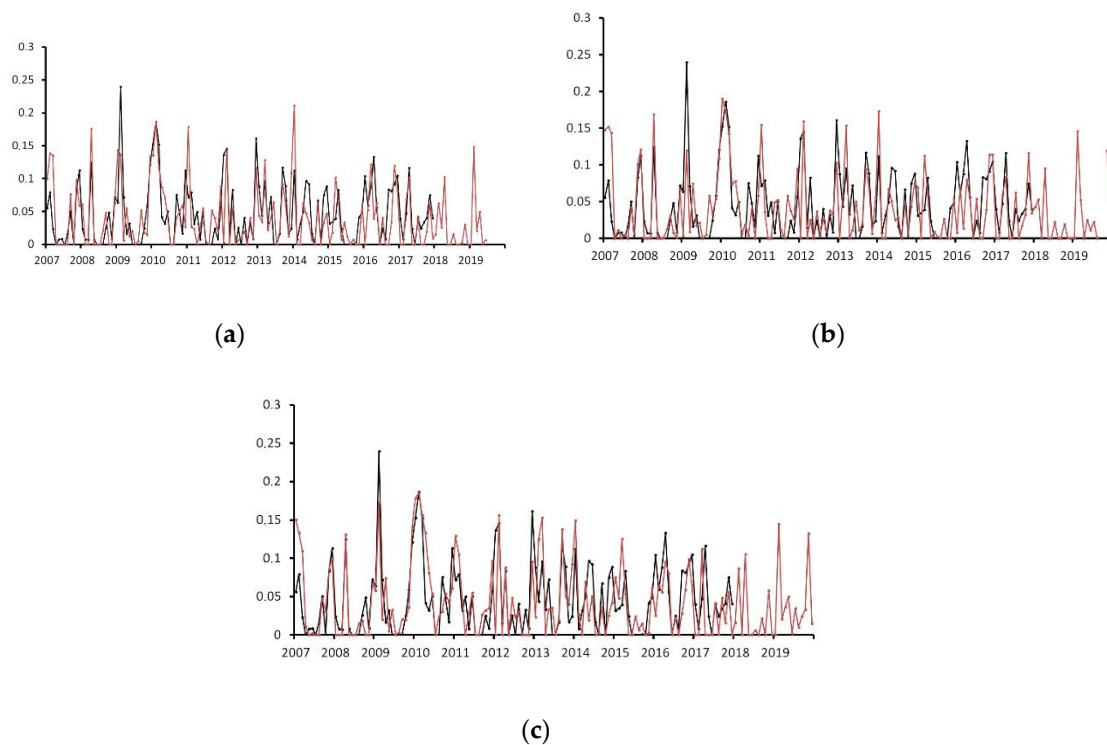


Figure 8. Annual time series of the calculated (black line) and simulated (red line) frequency (dimensionless values) of intense cyclones in the Black Sea region with a lead time of (a) 2, (b) 4 and (c) 6 months.

3.5. Case Studies of Regional Manifestations of Deep Cyclones in the Types of Storms in the Northern Black Sea Coast

We conducted the analysis of composite maps of centers of cyclones in the days of storms from data set #1, full storm tracks from data set #2, sea level pressure, 1000 hPa and 500 hPa geopotential height and 1000 hPa wind vector for the selected four types (1b, 2a, 2b and 3) of storminess according to [15] associated with wave heights of no less than 5 m at the northern Black Sea coast.

The storm type 1b (13 events) was characterized mainly by storm tracks crossing the Black Sea from southwest (SW) to northeast (NE) with deep centers of cyclones on the dates of storms located along this line and focused in the northern sector of the region. Minimum SLP less than 1010 hPa was located to the north of Crimea, as was minimal 1000 hPa geopotential height lower than 85 hPa, albeit slightly shifted to northeast. The west of the northern Black Sea coast was occupied by a trough in the field of 500 hPa geopotential height and southeastward 1000 hPa wind vector.

For the storm type 2a (17 events), storm tracks were located along the same line from SW to NE, but shifted to the north/northwest of the northern Black Sea coast, which was especially noticeable for deep cyclonic centers on the dates of storms. Locations of the minimal SLP and 1000 hPa geopotential height were generally the same as for the previous type 1b, but with a substantially lower central value: <1004 hPa for SLP and <10 m for geopotential height. A southern edge of this center over the northern Black Sea coast was characterized by the NW–SE direction of a 1000 hPa wind vector and 500 hPa geopotential height gradient.

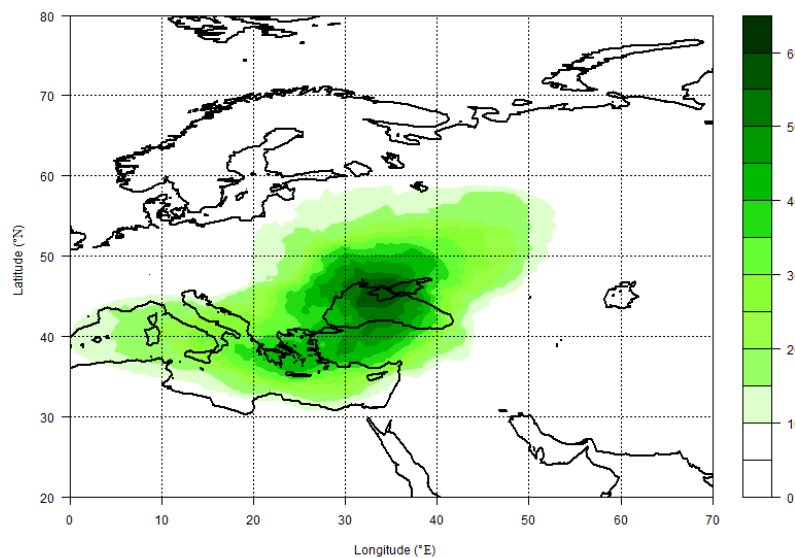
While full storm tracks for the type 2b (10 events) were identified to the north and east of the Black Sea, majority of them were located to the northeast of the northern Black Sea coast. Most deep centers of cyclones on the dates of storms were located in the northeastern sector, unlike the two previous types (1b and 2a). Areas of minimal values of SLP, 1000 hPa and 500 hPa geopotential height, were located to the NE of the northern Black Sea coast, falling below 1004 hPa for the SLP, 30 m for the 1000 hPa geopotential height and 5200 m for the 500 hPa geopotential height (the lowest values in comparison

with the previous types 1b and 2a). The direction of 1000 hPa wind vector was southeastward along the entire northern Black Sea coast.

The last storm type described here, type 3, included the least number of cases (5 events) but was still characterized by relatively dense frequency of full storm tracks and deep centers of cyclones on the dates of storms concentrated to the southeast of the Black Sea, where the areas of minimum values of the SLP (lower 1011 hPa) and 1000 hPa geopotential height (lower 90 m) were located as well. The minimal 500 hPa geopotential height was located over the NW Black Sea shelf. The 1000 hPa wind vector was mostly westward over the northern Black Sea coast.

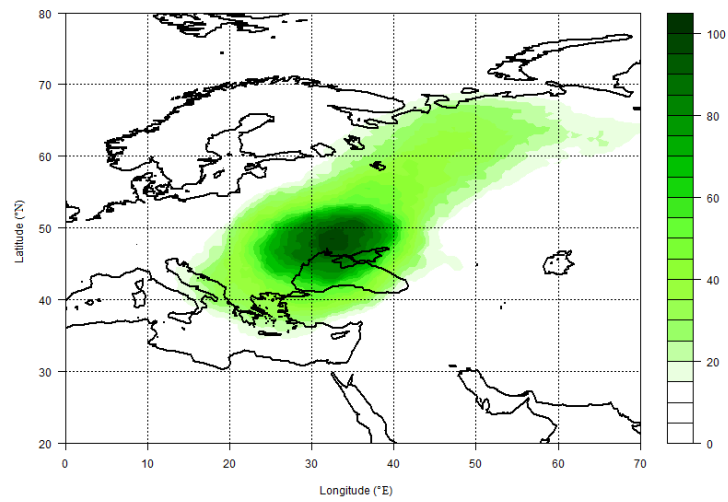
Taking into account the geometry of cyclones (their entire area) from the data set #2, the composite maps of the frequency of cyclones as closed systems were obtained (Figure 9). The maps, grouped for these four storm types, show the frequency of passage of the entire area of a cyclone through a specific space point. Maximum passage frequency of the total number of cyclones for type 1b was located over the Crimean peninsula (Figure 9a), for type 2a to the north–northwest of the Black Sea coast (Figure 9b), for type 2b to the northeast (Figure 9c) and for type 3 to the south–southeast (Figure 9d).

These results obtained for the groups of severest storms (with wave heights equal to or higher than 5 m) agree with the early results by Chernyakova et al. [84,85] for separate storms in 1965–69, where baric fields and position of synoptic systems were shown for different stormy wind directions over the Black Sea. Two types of storm fields of atmospheric pressure with the position of the cyclonic center to the north or south of the Black Sea were distinguished recently in paper [86]. Our case studies showed that types of storms with wave height higher than or equal to 5 m over the northern Black Sea coast were associated with groups of centers of deep cyclones located relative to this coast in the north (type 1b), northwest (type 2a), northeast (type 2b) and southeast (type 3).

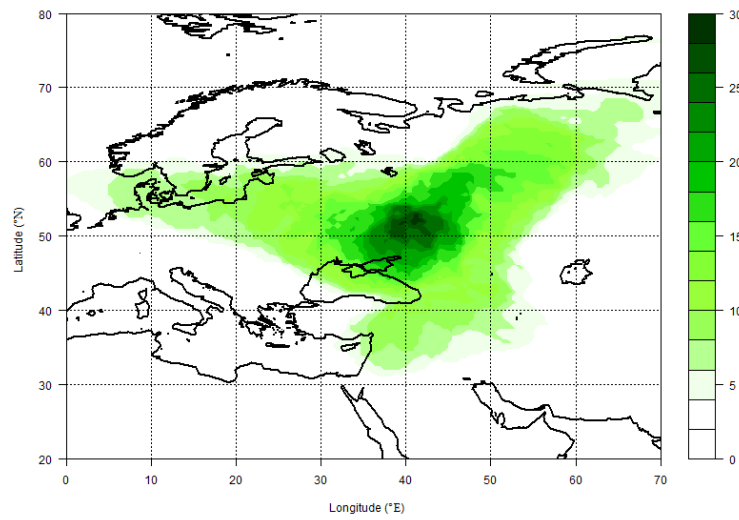


(a)

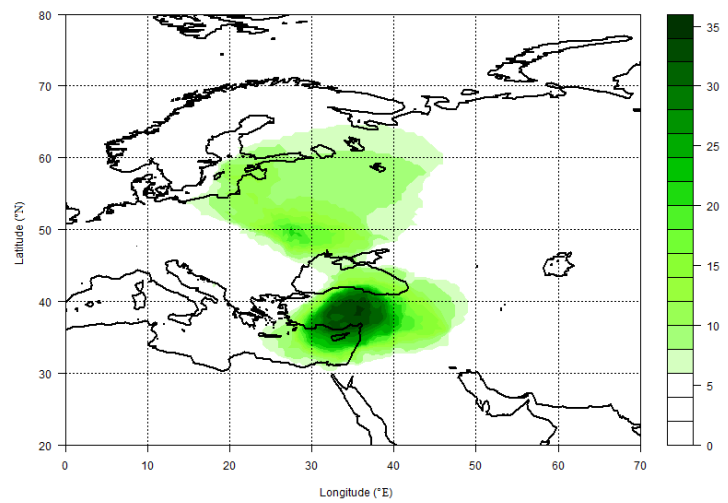
Figure 9. Cont.



(b)



(c)



(d)

Figure 9. Composite maps of the passage frequencies of cyclones as closed systems from data set #2 for the storm types: (a) type 1b, (b) type 2a, (c) type 2b, (d) type 3.

4. Conclusions

This study was carried out as a part of ongoing research of regional climatic–environmental anomalies in the Black Sea region. Earlier papers were devoted to the total number of cyclones in the region [23,42,70] or individual cases of intense cyclones [40], but not to their climatology. The focus of this study was on the long-term variability of the frequency of deep cyclones, which have an important socioeconomic impact. Intense cyclones were identified as the 0.75 quantile and extreme cyclones as the 0.95 quantile of the total number of cyclones (while the variability of intense cyclones includes the variability of extreme cyclones). We studied the characteristics and described the peculiarities of their seasonal and interannual–interdecadal variability in the terms of conventional statistical and spectral analysis, tested the possibility of their predictability using the developed model of neural networks and studied their relationship with the types of storminess on the northern Black Sea coast.

It was shown that the frequency of deep cyclones identified by the depth was higher in all seasons than that identified by intensity, because the depth of cyclones in our study did not take into account their area (and consequently a gradient) in contrast to intensity. The highest values of the frequency of deep cyclones were in winter, with a maximum in February (except for the maximum of standard deviation of the frequency of intense cyclones in January), and the lowest (or close to zero for extreme cyclones) were in summer, with a minimum in August, with the 6–8 times difference between the maximum and minimum for intense cyclones. A feature of the annual cycle of extreme cyclones is a steeper descending frequency from winter to spring months. Variability of extreme cyclones has a higher contribution of interannual amplitude to the total variance than that of intense cyclones.

The most prominent feature of variability of annual values of deep cyclones was a peak in the mid-1960s (up to 3σ standardized anomalies for intense cyclones and 2.5σ for extreme cyclones), mostly pronounced in winter and also in spring for the intense cyclones. It was followed by a decrease until the 1990s (lower 1σ), during which autumn frequencies of deep cyclones were low or negligible, and the period of increase after that up to the end of the time interval (mostly due to winter). Low frequency variability after 14 years filtering was characterized by the periodicity of about 35 years. It is possible that the end of the time interval (2017) was characterized by the transition from negative to positive annual anomalies of the frequency of deep cyclones on the background of sustainable growth of the interdecadal residuals (≥ 14 years) of variability of anomalies.

Negative linear trends for the annual frequency of deep cyclones were estimated as significant at the level of 97.5% for intense cyclones (coefficient of determination $R^2 = 7.3\%$) due to winter and spring and at the level of 92.4% for extreme cyclones ($R^2 = 4.8\%$) due to winter. The contribution of the low-frequency component (≥ 14 years) to variance of the annual values (R^2) reached more than 53% (60% with the contribution of linear trend) for the frequency of intense cyclones (mainly due to winter and spring) and more than 33% (38%, respectively) for the frequency of extreme cyclones (due to winter). As for the contribution of high-frequency variability, a summer–autumn maximum of 81–96% for intense cyclones, as well as a spring one for extreme cyclones, was observed, while the contribution of the high-frequency component to the annual variance reached 39.4% and 61.5%, respectively.

Spectral analysis of the high-frequency component (up to 14 years) of the seasonal and annual frequency of deep cyclones showed a descending spectrum for intense cyclones and an ascending one for extreme cyclones, which indicates that for extreme cyclones more energy was concentrated at higher frequencies, while for intense cyclones at lower frequencies. Typical periods of interannual variability were identified as 2.5/2.4 and 7.7/5.6, 3.4 years for intense cyclones (due to spring contribution)/extreme cyclones (due to winter contribution).

Modeling using neural networks allows successful forecasting of the frequency of intense cyclones in the Black Sea region, with a lead time of up to 6 months for all months except December–January and July–August (probably due to the different set of predictors and higher standard deviations as compared with the mean values these months). Consequently, there is a potential of the neural network modeling for forecasting cyclones in the Black Sea region.

Case studies of the role of deep cyclones in the generation of storms with wave heights above 5 m in the northern Black Sea coast showed that the types of storms were associated with specific baric situations when deep cyclone centers were concentrated in the north (type 1b), northwest (type 2a), northeast (type 2b) and southeast (type 3) of the Black Sea coast.

The key findings, which are of the greatest practical interest for the sustainable development of the studied region, can be outlined as follows:

- The highest frequency of intense cyclones is from November to May, while for extreme cyclones this period is from November to March with the maximum in February for the both;
- When characterizing the regime and variability of deep cyclones in the region, it is necessary to take into account significant linear trends for some seasons (which are responsible for up to 10% contribution to dispersion in winter), as well as the low-frequency component of variability (which makes up to half of the contribution to dispersion for extreme cyclones in winter and more than half of the contribution to dispersion for intense cyclones in winter and spring);
- Typical periods of interannual variability of winter–spring deep cyclones are about 2.5–3.5 and 6–8 years, the same as for the North Atlantic Oscillation and El Nino–Southern Oscillation;
- The neural network modeling for forecasting cyclones in the region is a promising approach and requires a separate study;
- The plausible pattern of the distribution of deep cyclone centers associated with the types of storms on the northern Black Sea coast is shown.

The outlook for further research of intense cyclones in the Black Sea region is important, not only in terms of developing the theory of long-term forecasts of weather and climate anomalies (based on the patterns of regional manifestations of large-scale processes in the ocean–atmosphere system), but also for solving the applied problems of long-term planning of regional sustainable development under climate change. Examples include a number of developed projects and activities for solving urgent regional problems, taking into account trends and natural patterns of change of dangerous hydrometeorological phenomena. They concern protecting and strengthening coasts, risk management of the coastal zone, prevention of emergencies of technogenic and environmental problems, long-term perspective planning of safe activities of the recreational, agricultural, mining sectors, the city’s fresh water sector (taking into account the level of reservoir filling), seaports and engineering structures.

Author Contributions: Conceptualization, V.N.M. and E.N.V.; data curation, A.V.Y.; formal analysis, V.N.M., A.S.L., A.V.Y., and V.Y.Z.; funding acquisition, V.N.M.; investigation, V.N.M.; methodology, A.S.L., A.V.Y., and V.Y.Z.; project administration, V.N.M. and E.N.V.; software, A.S.L., A.V.Y., V.Y.Z., and V.P.E.; supervision, E.N.V.; visualization, V.N.M., A.S.L., A.V.Y., and V.Y.Z.; writing—original draft, V.N.M., A.S.L., and V.Y.Z.; writing—review and editing, E.N.V. and V.P.E. All authors have read and agreed to the published version of the manuscript.

Funding: This research was funded by RFBR and the Government of the Sevastopol according to the research project № 18-41-920068 and by the state assignment of the Institute of Natural Technical Systems within the research theme № 0012-2019-0007.

Acknowledgments: The authors acknowledge M.Y. Bardin, Institute of Global Climate and Ecology, Institute of Geography of the Russian Academy of Sciences, Moscow, for methodological support.

Conflicts of Interest: The authors declare no conflict of interest. The funders had no role in the design of the study; in the collection, analyses, or interpretation of data; in the writing of the manuscript; or in the decision to publish the results.

Appendix A

Table A1. Table of acronyms of reanalysis.

Acronym	Meaning
NCEP/NCAR	A joint product from the National Centers for Environmental Prediction (NCEP) and the National Center for Atmospheric Research (NCAR)
ERA	European Centre for Medium-Range Weather Forecasts (ECMWF) reanalysis
JRA	The Japanese global atmospheric reanalysis by the Japan Meteorological Agency (JMA)
MERRA	Modern-era retrospective analysis for research and applications
20CR	Twentieth century reanalysis project

References

- Gopalakrishnan, T.; Hasan, M.K.; Haque, A.; Jayasinghe, S.L.; Kumar, L. Sustainability of Coastal Agriculture under Climate Change. *Sustainability* **2019**, *11*, 7200. [[CrossRef](#)]
- Kemp-Benedict, E.; Lamontagne, J.; Laing, T.; Drakes, C. Climate Impacts on Capital Accumulation in the Small Island State of Barbados. *Sustainability* **2019**, *11*, 3192. [[CrossRef](#)]
- Ahmed, B.; Kelman, I.; Fehr, H.K.; Saha, M. Community Resilience to Cyclone Disasters in Coastal Bangladesh. *Sustainability* **2016**, *8*, 805. [[CrossRef](#)]
- Fink, A.H.; Pohle, S.; Pinto, J.G.; Knippertz, P. Diagnosing the influence of diabatic processes on the explosive deepening of extratropical cyclones. *Geophys. Res. Lett.* **2012**, *39*. [[CrossRef](#)]
- Pirret, J.S.; Knippertz, P.; Trzeciak, T.M. Drivers for the deepening of severe European windstorms and their impacts on forecast quality. *Q. J. R. Meteorol. Soc.* **2017**, *143*, 309–320. [[CrossRef](#)]
- Zappa, G.; Shaffrey, L.C.; Hodges, K.I.; Sansom, P.G.; Stephenson, D.B. A Multimodel Assessment of Future Projections of North Atlantic and European Extratropical Cyclones in the CMIP5 Climate Models. *J. Clim.* **2013**, *26*, 5846–5862. [[CrossRef](#)]
- Akperov, M.; Bardin, M.Y.; Volodin, E.; Golitsyn, G.; Mokhov, I. Probability distributions for cyclones and anticyclones from the NCEP/NCAR reanalysis data and the INM RAS climate model. *Izv. Atmos. Ocean. Phys.* **2007**, *43*, 705–712. [[CrossRef](#)]
- Toptunova, O.; Aniskina, O. Cyclone regime in the Northern and Southern Hemisphere. In Proceedings of the International Scientific and Practical Conference World Science, Ajman, UAE, 22–23 November 2015; pp. 74–78.
- Baatsen, M.; Haarsma, R.J.; Van Delden, A.J.; de Vries, H. Severe Autumn storms in future Western Europe with a warmer Atlantic Ocean. *Clim. Dyn.* **2015**, *45*, 949–964. [[CrossRef](#)]
- Nesterov, E.S. *Extreme Cyclones in the Atlantic-European Region*; Hydrometeorological Center of Russia: Moscow, Russia, 2018; p. 104.
- Luksch, U.; Raible, C.C.; Blender, R.; Fraedrich, K. Decadal cyclone variability in the North Atlantic. *Meteorol. Z.* **2005**, *14*, 747–753. [[CrossRef](#)]
- Geng, Q.Z.; Sugi, M. Variability of the North Atlantic cyclone activity in winter analyzed from NCEP-NCAR reanalysis data. *J. Clim.* **2001**, *14*, 3863–3873. [[CrossRef](#)]
- Zolina, O.; Gulev, S.K. Improving the accuracy of mapping cyclone numbers and frequencies. *Mon. Weather Rev.* **2002**, *130*, 748–759. [[CrossRef](#)]
- Rudeva, I.; Gulev, S.K. Composite analysis of North Atlantic extratropical cyclones in NCEP-NCAR reanalysis data. *Mon. Weather Rev.* **2011**, *139*, 1419–1446. [[CrossRef](#)]
- Polonsky, A.; Evstigneev, V.; Naumova, V.; Voskresenskaya, E. Low-frequency variability of storms in the northern Black Sea and associated processes in the ocean-atmosphere system. *Reg. Environ. Chang.* **2014**, *14*, 1861–1871. [[CrossRef](#)]
- Baltaci, H.; Akkoyunlu, B.O.; Tayanc, M. Relationships between teleconnection patterns and Turkish climatic extremes. *Theor. Appl. Climatol.* **2018**, *134*, 1365–1386. [[CrossRef](#)]
- Khromov, S.P.; Mamontova, L.I. *Meteorological Dictionary*; Gidrometeoizdat: Leningrad, Russia, 1974.
- Barnston, A.G.; Livezey, R.E. Classification, seasonality and persistence of low-frequency atmospheric circulation patterns. *Mon. Weather Rev.* **1987**, *115*, 1083–1126. [[CrossRef](#)]

19. Enfield, D.B.; Mestas-Nuñez, A.M. Multiscale variabilities in global sea surface temperatures and their relationships with tropospheric climate patterns. *J. Clim.* **1999**, *12*, 2719–2733. [[CrossRef](#)]
20. Wang, X.L.L.; Wan, H.; Zwiers, F.W.; Swail, V.R.; Compo, G.P.; Allan, R.J.; Vose, R.S.; Jourdain, S.; Yin, X.G. Trends and low-frequency variability of storminess over western Europe, 1878–2007. *Clim. Dyn.* **2011**, *37*, 2355–2371. [[CrossRef](#)]
21. Matulla, C.; Schoner, W.; Alexandersson, H.; von Storch, H.; Wang, X.L. European storminess: Late nineteenth century to present. *Clim. Dyn.* **2008**, *31*, 125–130. [[CrossRef](#)]
22. Wang, X.L.L.; Zwiers, F.W.; Swail, V.R.; Feng, Y. Trends and variability of storminess in the Northeast Atlantic region, 1874–2007. *Clim. Dyn.* **2009**, *33*, 1179–1195. [[CrossRef](#)]
23. Polonskii, A.B.; Bardin, M.Y.; Voskresenskaya, E.N. Statistical characteristics of cyclones and anticyclones over the Black Sea in the second half of the 20th century. *Phys. Oceanogr.* **2007**. [[CrossRef](#)]
24. Krasnyuk, T.V.; Nesterov, E.S. Characteristics of deep cyclones and extreme waves in the North Atlantic from the ERA-Interim reanalysis data. *Russ. Meteorol. Hydrol.* **2015**, *40*, 191–198. [[CrossRef](#)]
25. Nesterov, E.S. On the influence of North Atlantic and East Atlantic fluctuations on the formation of dangerous waves in the North Atlantic. *Proc. Hydrometeorol. Res. Cent. Russ. Fed.* **2016**, *362*, 83–91.
26. Comas-Bru, L.; McDermott, F. Impacts of the EA and SCA patterns on the European twentieth century NAO-winter climate relationship. *Q. J. R. Meteorol. Soc.* **2014**, *140*, 354–363. [[CrossRef](#)]
27. Nesterov, E.S. Variability of atmospheric and ocean characteristics in the Atlantic-European region during the El Niño and La Niña events. *Russ. Meteorol. Hydrol.* **2000**, 74–83.
28. Gushchina, D.; Dewitte, B. *El Niño Southern Oscillation and Its Influence on the Ocean-Atmosphere Processes*; State Oceanographic Institute Proceedings: Moscow, Russia, 2016; pp. 184–208.
29. Zheleznova, I.V.; Gushchina, D.Y. Circulation anomalies in the atmospheric centers of action during the Eastern Pacific and Central Pacific El Niño. *Russ. Meteorol. Hydrol.* **2016**, *41*, 760–769. [[CrossRef](#)]
30. Voskresenskaya, E.N.; Marchukova, O.V.; Maslova, V.N.; Lubkov, A.S. Interannual climate anomalies in the Atlantic-European region associated with La-Nina types. In Proceedings of the 3rd International Conference on Environment and Sustainable Development of Territories—Ecological Challenges of the 21st Century, Kazan, Russia, 27–29 September 2017.
31. Voskresenskaya, E.N.; Polonskii, A.B. Trends and interannual variability of parameters of large-scale air-sea interaction in the North Atlantic. *Oceanogr. Lit. Rev.* **1995**, *12*, 1057.
32. Tilinina, N.; Gulev, S.K.; Rudeva, I.; Koltermann, P. Comparing cyclone life cycle characteristics and their interannual variability in different reanalyses. *J. Clim.* **2013**, *26*, 6419–6438. [[CrossRef](#)]
33. Rudeva, I.A. Life cycle of atmospheric extratropical cyclones of the Northern Hemisphere and its relationship with the processes of interaction between the ocean and the atmosphere. *Izv. Atmos. Ocean. Phys.* **2008**, *44*, 1–7.
34. Sanders, F.; Gyakum, J.R. Synoptic-dynamic climatology of the “bomb”. *Mon. Weather Rev.* **1980**, *108*, 1589–1606. [[CrossRef](#)]
35. Wirth, V.; Eichhorn, J. Long-lived Rossby wave trains as precursors to strong winter cyclones over Europe. *Q. J. R. Meteorol. Soc.* **2014**, *140*, 729–737. [[CrossRef](#)]
36. Zimin, A.V.; Szunyogh, I.; Patil, D.J.; Hunt, B.R.; Ott, E. Extracting envelopes of Rossby wave packets. *Mon. Weather Rev.* **2003**, *131*, 1011–1017. [[CrossRef](#)]
37. Mailier, P.J.; Stephenson, D.B.; Ferro, C.A.T.; Hodges, K.I. Serial clustering of extratropical cyclones. *Mon. Weather Rev.* **2006**, *134*, 2224–2240. [[CrossRef](#)]
38. Pinto, J.G.; Bellenbaum, N.; Karremann, M.K.; Della-Marta, P.M. Serial clustering of extratropical cyclones over the North Atlantic and Europe under recent and future climate conditions. *J. Geophys. Res. Atmos.* **2013**, *118*, 12476–12485. [[CrossRef](#)]
39. Vitolo, R.; Stephenson, D.B.; Cook, I.M.; Mitchell-Wallace, K. Serial clustering of intense European storms. *Meteorol. Z.* **2009**, *18*, 411–424. [[CrossRef](#)]
40. Lopatukhin, L.; Bukhanovsky, A.; Chernysheva, E.; Kolesov, A. About the storm in the Black Sea in November 2007. In *Russian River Register*; Publishing Center “Academy”: St. Petersburg, Russia, 2009; p. 35.
41. Trigo, I.F.; Bigg, G.R.; Davies, T.D. Climatology of cyclogenesis mechanisms in the Mediterranean. *Mon. Weather Rev.* **2002**, *130*, 549–569. [[CrossRef](#)]
42. Maslova, V.; Voskresenskaya, E.; Bardin, M. Variability of the cyclone activity in the Mediterranean-Black Sea region. *J. Environ. Prot. Ecol.* **2010**, *11*, 1366–1372.

43. Neu, U.; Akperov, M.G.; Bellenbaum, N.; Benestad, R.S.; Blender, R.; Caballero, R.; Coccozza, A.; Dacre, H.F.; Feng, Y.; Fraedrich, K.; et al. IMILAST: A Community Effort to Intercompare Extratropical Cyclone Detection and Tracking Algorithms. *Bull. Am. Meteorol. Soc.* **2013**, *94*, 529–547. [[CrossRef](#)]
44. Alexandersson, H.; Tuomenvirta, H.; Schmith, T.; Iden, K. Trends of storms in NW Europe derived from an updated pressure data set. *Clim. Res.* **2000**, *14*, 71–73. [[CrossRef](#)]
45. Krueger, O.; von Storch, H. Evaluation of an air pressure-based proxy for storm activity. *J. Clim.* **2011**, *24*, 2612–2619. [[CrossRef](#)]
46. Akperov, M.G.; Mokhov, I.I. A comparative analysis of the method of extratropical cyclone identification. *Izv. Atmos. Ocean. Phys.* **2010**, *46*, 620–637. [[CrossRef](#)]
47. Lionello, P.; Trigo, I.F.; Gil, V.; Liberato, M.L.R.; Nissen, K.M.; Pinto, J.G.; Raible, C.C.; Reale, M.; Tanzarella, A.; Trigo, R.M.; et al. Objective climatology of cyclones in the Mediterranean region: A consensus view among methods with different system identification and tracking criteria. *Tellus Ser. A-Dyn. Meteorol. Oceanogr.* **2016**, *68*, 18. [[CrossRef](#)]
48. Kalnay, E.; Kanamitsu, M.; Kistler, R.; Collins, W.; Deaven, D.; Gandin, L.; Iredell, M.; Saha, S.; White, G.; Woollen, J.; et al. The NCEP/NCAR 40-year reanalysis project. *Bull. Am. Meteorol. Soc.* **1996**, *77*, 437–471. [[CrossRef](#)]
49. Bardin, M.Y. Variability of cyclonicity characteristics in the middle troposphere of temperate latitudes of the Northern Hemisphere. *Russ. Meteorol. Hydrol.* **1995**, *11*, 24–37.
50. Haylock, M.R.; Goodess, C.M. Interannual variability of european extreme winter rainfall and links with mean large-scale circulation. *Int. J. Climatol.* **2004**, *24*, 759–776. [[CrossRef](#)]
51. Zhuravsky, V.Y.; Voskresenskaya, E.N. Technology of cyclones separation from global reanalyses data sets on meteorological fields. *Monit. Syst. Environ.* **2018**. [[CrossRef](#)]
52. Wahba, G. Spline interpolation and smoothing on the sphere. *Siam J. Sci. Stat. Comput.* **1981**, *2*, 5–16. [[CrossRef](#)]
53. Howell, K.B. *Principles of Fourier Analysis*; CRC Press: Boca Raton, FL, USA, 2016.
54. Parzen, E. On estimation of a probability density function and mode. *Ann. Math. Stat.* **1962**, *33*, 1065–1076. [[CrossRef](#)]
55. Wallace, J.M.; Gutzler, D.S. Teleconnections in the geopotential height field during the northern hemisphere winter. *Mon. Weather Rev.* **1981**, *109*, 784–812. [[CrossRef](#)]
56. Mo, K.C.; White, G.H. Teleconnections in the southern-hemisphere. *Mon. Weather Rev.* **1985**, *113*, 22–37. [[CrossRef](#)]
57. Trenberth, K.E.; Caron, J.M. The Southern Oscillation revisited: Sea level pressures, surface temperatures, and precipitation. *J. Clim.* **2000**, *13*, 4358–4365. [[CrossRef](#)]
58. Osovsky, S. *Neural Networks for Data Processing*; Finansy i statistika: Moscow, Russia, 2004; p. 344.
59. Haykin, S. *Neural Networks: A Comprehensive Foundation*; Prentice Hall PTR: Upper Saddle River, NJ, USA, 1994.
60. Lubkov, A.; Voskresenskaya, E.; Kukushkin, A. Method for reconstructing the monthly mean water transparencies for the northwestern part of the Black Sea as an example. *Atmos. Ocean. Opt.* **2016**, *29*, 457–464. [[CrossRef](#)]
61. Lubkov, A.S.; Voskresenskaya, E.N.; Marchukova, O.V. Application of a neural network model to forecasting of El Niño and La Niña. In Proceedings of the IOP Conference Series: Earth and Environmental Science, Moscow, Russian, 27 May–6 June 2019; p. 012040.
62. Katz, A.A. *Seasonal Changes in General Atmospheric Circulation and Long-Term Forecasts*; Gydrometeoizdat: Leningrad, Russia, 1960.
63. Wangenheim, G.Y. On fluctuations in atmospheric circulation over the Northern Hemisphere. *Izv. Acad. Sci. Ussr. Geogr. Geophys. Ser.* **1946**, *5*, 405–416.
64. Girs, A.A. On the issue of studying the basic forms of atmospheric circulation. *Sov. Meteorol. Hydrol.* **1948**, *3*, 9–21.
65. Osuchowska-Klein, B. *Katalog Typów Cyrkulacji Atmosferycznej, 1976–1990*; IMGW: Warszawa, Poland, 1978.
66. Baur, F.; Hess, P.; Nagel, H. Kalender der grosswetterlagen Europas 1881–1939. Bad Homburg, Germany, 1944; Volume 35.
67. Hess, P.; Brezowsky, H. Katalog der Großwetterlagen Europas. *Ber. Dt. Wetterd.* **1969**, *15*, 56.
68. Werner, P.C.; Gerstengarbe, F.W. Katalog der Großwetterlagen Europas. *PIK Rep.* **2010**, *119*, 140.

69. Leckebusch, G.C.; Weimer, A.; Pinto, J.G.; Reyers, M.; Speth, P. Extreme wind storms over Europe in present and future climate: A cluster analysis approach. *Meteorol. Z.* **2008**, *17*, 67–82. [[CrossRef](#)]
70. Voskresenskaya, E.N.; Maslova, V.N. Winter-spring cyclonic variability in the Mediterranean-Black Sea region associated with global processes in the ocean-atmosphere system. *Adv. Sci. Res.* **2011**, *6*, 237–243. [[CrossRef](#)]
71. Novikova, A.; Polonskii, A. Inter-decadal variability of the Black Sea surface and cold intermediate layer temperature. *Monit. Syst. Environ.* **2018**. [[CrossRef](#)]
72. McCabe, G.J.; Clark, M.P.; Serreze, M.C. Trends in Northern Hemisphere surface cyclone frequency and intensity. *J. Clim.* **2001**, *14*, 2763–2768. [[CrossRef](#)]
73. Polonsky, A.B.; Voskresenskaya, E.N.; Naumova, V.A. Climatic anomalies; Black Sea hurricanes and environmental conditions. *Bull. Black Sea Comm.* **2008**, *14*, 3–5. [[CrossRef](#)]
74. Galabov, V.; Chervenkov, H. Study of the Western Black Sea storms with a focus on the storms caused by cyclones of North African origin. *Pure Appl. Geophys.* **2018**, *175*, 3779–3799. [[CrossRef](#)]
75. Zainescu, F.; Vespremeanu-Stroe, A. Storm climate and morphological imprints on the Danube delta coast. In *Landform Dynamics and Evolution in Romania*; Radoane, M., VespremeanuStroe, A., Eds.; Springer International Publishing Ag: Cham, Switzerland, 2017; pp. 845–865. [[CrossRef](#)]
76. Zainescu, F.I.; Tatui, F.; Valchev, N.N.; Vespremeanu-Stroe, A. Storm climate on the Danube delta coast: Evidence of recent storminess change and links with large-scale teleconnection patterns. *Nat. Hazards* **2017**, *87*, 599–621. [[CrossRef](#)]
77. Efimov, V.; Anisimov, A. Climatic parameters of wind-field variability in the Black Sea region: Numerical reanalysis of regional atmospheric circulation. *Izv. Atmos. Ocean. Phys.* **2011**, *47*, 350–361. [[CrossRef](#)]
78. Seip, K.L.; Gron, O. On the statistical nature of distinct cycles in global warming variables. *Clim. Dyn.* **2019**, *52*, 7329–7337. [[CrossRef](#)]
79. Gamiz-Fortis, S.R.; Pozo-Vazquez, D.; Esteban-Parra, M.J.; Castro-Diez, Y. Spectral characteristics and predictability of the NAO assessed through Singular Spectral Analysis. *J. Geophys. Res. Atmos.* **2002**, *107*, 15. [[CrossRef](#)]
80. Moron, V.; Ward, M.N. ENSO teleconnections with climate variability in the European and African sectors. *Weather* **1998**, *53*, 287–295. [[CrossRef](#)]
81. Bronnimann, S. Impact of El Nino Southern Oscillation on European climate. *Rev. Geophys.* **2007**, *45*, 28. [[CrossRef](#)]
82. Pozo-Vázquez, D.; Esteban-Parra, M.J.; Rodrigo, F.S.; Castro-Diez, Y. The association between ENSO and winter atmospheric circulation and temperature in the North Atlantic region. *J. Clim.* **2001**, *14*, 3408–3420. [[CrossRef](#)]
83. Cassou, C.; Terray, L. Oceanic forcing of the wintertime low-frequency atmospheric variability in the North Atlantic European sector: A study with the ARPEGE model. *J. Clim.* **2001**, *14*, 4266–4291. [[CrossRef](#)]
84. Chernyakova, A.P. Northeastern storms in the Black and Azov Seas during the movement of cyclones from Asia Minor to the southeast of the Black Sea. *Collect. Sci. Pap. Ukr. Res. Hydrometeorol. Inst.* **1958**, *12*, 123–132.
85. Chernyakova, A.P. Typical Black Sea wind fields. *Collect. Work. Basin Hydrometeorol. Obs. Black Azov Seas* **1965**, *3*, 25–27.
86. Surkova, G.V.; Koltermann, K.P.; Kislov, A.V. Method of forecasting storm conditions for the Black Sea under climate changes. *Mosc. Univ. Bull. Ser.5 Geogr.* **2012**, *6*, 25–31.

